Signal and noise separation in prestack seismic data using velocity-dependent seislet transform[a]

[a]Published in Geophysics, 80, no. 6, WD117-WD128, (2015)

Yang Liu, Sergey Fomel†, Cai Liu**

ABSTRACT

The seislet transform is a wavelet-like transform that analyzes seismic data by following varying slopes of seismic events across different scales and provides a multiscale orthogonal basis for seismic data. It generalizes the discrete wavelet transform (DWT) in the sense that DWT in the lateral direction is simply the seislet transform with a zero slope. Our earlier work used plane-wave destruction (PWD) to estimate smoothly varying slopes. However, PWD operator can be sensitive to strong noise interference, which makes the seislet transform based on PWD (PWD-seislet transform) occasionally fail in providing a sparse multiscale representation for seismic field data. We adopt a new velocity-dependent (VD) formulation of the seislet transform, where the normal moveout equation serves as a bridge between local slope patterns and conventional moveout parameters in the common-midpoint (CMP) domain. The velocity-dependent (VD) slope has better resistance to strong random noise, which indicates the potential of VD seislets for random noise attenuation under 1D earth assumption. Different slope patterns for primaries and multiples further enable a VD-seislet frame to separate primaries from multiples when the velocity models of primaries and multiples are well disjoint. Results of applying the method to synthetic and field-data examples demonstrate that the VD-seislet transform can help in eliminating strong random noise. Synthetic and field-data tests also show the effectiveness of the VD-seislet frame for separation of primaries and pegleg multiples of different orders.

INTRODUCTION

Signal and noise separation is a persistent problem in seismic exploration. Sometimes noise is divided into random noise and coherent noise. Many authors have developed effective methods of eliminating random noise. Ristau and Moon (2001) compared several adaptive filters, which they applied in an attempt to reduce random noise in geophysical data. Karsli et al. (2006) applied complex-trace analysis to seismic data for random-noise suppression, recommending it for low-fold seismic data. Some transform methods were also used to deal with seismic random noise, e.g., the discrete cosine transform (Lu and Liu, 2007), the curvelet transform (Neelamani et al., 2008), and the seislet transform (Fomel and Liu, 2010). If seismic events are planar (lines

in 2D data and planes in 3D data) or locally planar, one can predict seismic events by using prediction techniques in the f-x domain (Canales, 1984; Sacchi and Kuehl, 2001; Liu and Liu, 2013) or the t-x domain (Claerbout, 1992; Fomel, 2002; Sacchi and Naghizadeh, 2009; Liu et al., 2015).

Multiple reflections are one kind of coherent noise, especially in marine environments. Wave-equation based algorithms for attenuating multiples have rapidly developed since 1990s and usually consist of two steps, namely multiple prediction (Verschuur et al., 1992; Berkhout and Verschuur, 1997; Weglein et al., 1997) and adaptive subtraction (Wang, 2003b; Guitton and Verschuur, 2004; Fomel, 2009a). However, these algorithms need to calculate a full wavefield, which is often a computational bottleneck for their application, especially in the 3D case. Another popular class of demultiple techniques is based on variants of the Radon transform (Foster and Mosher, 1992). Several revised Radon transforms have been proposed for multiple attenuation (Hunt et al., 1996; Zhou and Greenhalgh, 1996; Wang, 2003a; Hargreave et al., 2003). Radon-transform based methods often fail to provide accurate separation because of their non-sparsity in characterizing seismic data, although they can be improved by high-resolution methods (Sacchi and Ulrych, 1995; Herrmann et al., 2000; Trad et al., 2003). Despite their usual classification as noise, multiples can penetrate deeply enough into the subsurface to illuminate the prospect zone. In this sense, multiples can also be viewed as a viable signal, rather than noise (Reiter et al., 1991; Youn and Zhou, 2001; Berkhout and Verschuur, 2006). Brown and Guitton (2005) proposed a least-squares joint imaging of pegleg multiples and primaries and discussed separation of pegleg multiples and primaries in prestack data.

In seismic data analysis, it is common to represent signals as sums of plane waves by using multidimensional Fourier transforms. The discrete wavelet transform (DWT) is often preferred to the Fourier transform for characterizing digital images, because of its ability to localize events in both time and frequency domains (Jensen and la Cour-Harbo, 2001; Mallat, 2009). However, DWT may not be optimal for describing data that consist of plane waves. Wavelet-like transforms that explore directional characteristics of images have found important applications in seismic imaging and data analysis (Chauris and Nguyen, 2008; Herrmann et al., 2008). Fomel (2006) investigated the possibility of designing a wavelet-like transform tailored specifically to seismic data and introduced it as the seislet transform. Fomel and Liu (2010) further developed the seislet framework and proposed additional applications. The original 2D seislet transform utilizes local data slopes estimated by plane-wave destruction (PWD) filters (Fomel, 2002; Chen et al., 2013a,b). However, a PWD operator can be sensitive to strong interference, which makes the seislet transform based on PWD (PWD-seislet transform) occasionally fail in characterizing noisy signals.

In this paper, we develop a velocity-dependent (VD) concept (Liu and Liu, 2013), where local slopes in prestack data are evaluated from moveout parameters estimated by conventional velocity-analysis techniques. We implement a VD-seislet transform and propose its application for signal and noise separation. We expect the new VD-seislet transform to provide better compression ability for reflection events away from

interference of strong random noise. We also provide an application of VD-seislet transform for separating primaries from pegleg multiples of different orders. We test the performance of VD-seislet transform using synthetic and field data.

THEORY

Review of seislets

The seislet transform was introduced by Fomel (2006) and extended by Fomel and Liu (2010) and Liu and Fomel (2010). The seislet construction is based on the discrete wavelet transform (DWT) combined with seismic data patterns, such as local slopes or frequencies. Fomel (2002) developed a local plane-wave destruction (PWD) operation to predict local plane-wave events, where an all-pass digital filter is used to approximate the time shift between two neighboring traces. The inverse operation, plane-wave construction (Fomel and Guitton, 2006; Fomel, 2010), predicts a seismic trace from its neighbors by following locally varying slopes of seismic events and has been used for designing a PWD-seislet transform, which is a particular kind of the seislet transforms based on slope patterns. Liu and Liu (2013) proposed a velocity-dependent (VD) slope as a pattern in VD-seislet transform, where the normal moveout (NMO) equation serves as a bridge between local slopes and scanned NMO velocities.

To define seislet transform, we follow the general recipe of the lifting scheme for the discrete wavelet transform, as described by Sweldens and Schröder (1996). The construction is reviewed in Appendix A. Designing pattern-based prediction operator $\mathbf{P}$ and update operator $\mathbf{U}$ for seismic data is key in the seislet framework. In the seislet transform, the basic data components can be different, e.g., traces or common-offset gathers, and the prediction and update operators shift components according to different patterns.

The prediction and update operators for a simple seislet transform are defined by modifying the biorthogonal wavelet construction in equations from Appendix A as follows:

$$\mathbf{P}[\mathbf{e}]_k = \left(\mathbf{R}_k^{(+)}[\mathbf{e}_{k-1}] + \mathbf{R}_k^{(-)}[\mathbf{e}_k]\right)/2 \tag{1}$$

$$\mathbf{U}[\mathbf{r}]_k = \left(\mathbf{R}_k^{(+)}[\mathbf{r}_{k-1}] + \mathbf{R}_k^{(-)}[\mathbf{r}_k]\right)/4\ , \tag{2}$$

where $\mathbf{e}_k$ is even components of data at the kth transform scale, $\mathbf{r}_k$ is residual difference between the odd component of data $\mathbf{o}$ and its prediction from the even component at the kth transform scale, and $\mathbf{R}_k^{(+)}$ and $\mathbf{R}_k^{(-)}$ are operators that predict a component from its left and right neighbors correspondingly by shifting them according to their patterns. The details are explained in Appendix A.

To get the relationship between prediction operator $\mathbf{R}_k$ and slope pattern σ, the plane-wave destruction operation (Fomel, 2002) can be defined in a linear operator

notation as

$$\mathbf{d} = \mathbf{D}(\sigma)\,\mathbf{s}\;, \tag{3}$$

where seismic section $\mathbf{s} = [\mathbf{s}_1\ \mathbf{s}_2\ \ldots\ \mathbf{s}_N]^T$ is a collection of traces, and $\mathbf{d}$ is the destruction residual. The general structure of $\mathbf{D}$ is defined as follows (Fomel and Guitton, 2006; Fomel, 2010)

$$\mathbf{D}(\sigma) = \begin{bmatrix} \mathbf{I} & 0 & 0 & \cdots & 0 \\ -\mathbf{R}_{1,2}(\sigma_1) & \mathbf{I} & 0 & \cdots & 0 \\ 0 & -\mathbf{R}_{2,3}(\sigma_2) & \mathbf{I} & \cdots & 0 \\ \cdots & \cdots & \cdots & \cdots & \cdots \\ 0 & 0 & \cdots & -\mathbf{R}_{N-1,N}(\sigma_{N-1}) & \mathbf{I} \end{bmatrix}\;, \tag{4}$$

where $\mathbf{I}$ stands for the identity operator, σ_i is local slope pattern, and $\mathbf{R}_{i,j}(\sigma_i)$ is an operator for prediction of trace j from trace i according to the slope pattern σ_i. A trace is predicted by shifting it according to the local seismic event slopes. Prediction of a trace from a distant neighbor can be accomplished by simple recursion, i.e., predicting trace k from trace 1 is simply

$$\mathbf{R}_{1,k} = \mathbf{R}_{k-1,k}\,\cdots\,\mathbf{R}_{2,3}\,\mathbf{R}_{1,2}\;. \tag{5}$$

If $\mathbf{s}_r$ is a reference trace, then the prediction of trace $\mathbf{s}_k$ is $\mathbf{R}_{r,k}\mathbf{s}_r$.

The predictions need to operate at different scales, which, in this case, mean different separation distances between the data elements, e.g., traces in PWD-seislet transform. Equations 1 and 2, in combination with the forward and inverse lifting schemes, provide a complete definition of the seislet framework. For different kinds of slope-based seislets, one needs to define the corresponding slope pattern σ.

VD-slope pattern for primary reflections

The kinematic description of a seismic event is an essential step for several developments in seismic data processing. Local slope is one important kinematic pattern for seismic data in the time-space domain. PWD provides a constructive algorithm for estimating local slopes (Claerbout, 1992; Fomel, 2002; Schleicher et al., 2009; Chen et al., 2013a,b) and can combine with a seislet framework to implement the PWD-seislet. Local slant stack (Ottolini, 1983a) is another standard tool for calculating slopes.

Under 1D earth assumption, one can consider the classic hyperbolic model of primary reflection moveouts at near offsets (Dix, 1955):

$$t(x) = \sqrt{t_0^2 + \frac{x^2}{v^2(t_0)}}\;, \tag{6}$$

where t_0 is the zero-offset traveltime, $t(x)$ is the corresponding primary traveltime recorded at offset x, and $v(t_0)$ is the stacking, or root mean square (RMS) velocity,

which comes from a standard velocity scan. As follows from equation 6, the traveltime slopes $\sigma = dt/dx$ in CMP gathers are given by

$$\sigma(t,x) = \frac{x}{t(x)\, v^2(t_0,x)} \ . \tag{7}$$

This calculation is reverse to the one used in NMO by velocity-independent imaging (Ottolini, 1983b; Fomel, 2007). To calculate local slopes of primaries, we need to know $v(t_0,x)$ at each time-space location (t_0,x). This can be accomplished by simultaneously scanning both t_0 and $v(t_0,x)$ according to the hyperbolic NMO equation at each x-coordinate position or by *time-warping*. In this paper, we use the time-warping algorithm to calculate $v(t_0,x)$. Time warping performs mapping between different coordinates: if one has sampled functions $f(x)$ and $y(x)$, the mapping operation finds sampled $f(y)$ (Burnett and Fomel, 2009; Casasanta and Fomel, 2011).

After the VD-slope pattern of primaries is calculated, we can design pattern-based prediction and update operators $\mathbf{R}_k$ by using plane-wave construction for the VD-seislet transform to represent only primary reflections. When VD-seislet transform is applied to a CMP gather, random noise spreads over different scales while the predictable reflection information gets compressed to large coefficients at small scales. A simple thresholding operation can easily remove small coefficients. Finally, applying the inverse VD-seislet transform reconstructs the signal while attenuating random noise.

VD-slope pattern for pegleg multiples

In a laterally homogeneous model, the NMO equation 6 flattens primary events on a CMP gather with offset x and time t to its zero-offset traveltime t_0. Brown and Guitton (2005) use an analogous NMO equation for pegleg multiples under locally 1D earth assumption. For example, first-order pegleg can be kinematically approximated by pseudo-primary with the same offset but with an additional zero-offset traveltime τ. The NMO equation for an mth-order pegleg multiple is generalized to

$$t_m(x) = \sqrt{(t_0 + m\tau)^2 + \frac{x^2}{v_m^2(t_0)}} \ , \tag{8}$$

where $t_m(x)$ is the corresponding multiple traveltime recorded at offset x and the effective RMS velocity v_m is defined according to Dix's equation as:

$$v_m(t_0) = \sqrt{\frac{t_0 v^2(t_0) + m\tau\, v^2(\tau)}{t_0 + m\tau}} \ . \tag{9}$$

In marine seismic data, $v(\tau)$ is constant water velocity, and it assumes that we are able to pick zero-offset traveltime τ of the water bottom. According to the definition of slopes for primaries (equation 7), slopes for pegleg multiples can be calculated analogously by:

$$\sigma_m(t,x) = \frac{x}{t_m(x)\, v_m^2(t_0,x)} \ . \tag{10}$$

Equation 10 provides the estimation of multiple slopes, which we use to define VD-seislet frame for representing pegleg multiples of different orders.

Separation of primaries and pegleg multiples using VD-seislet frame

Once the VD-seislet transform is defined, it can be applied to analyze signals composed of multiple wavefields, e.g., primaries and multiples of different orders. If a range of slopes are chosen and a VD-seislet transform is constructed for each of them, then all the transforms together will constitute an overcomplete representation. Mathematically, if $\mathbf{F}_i$ is the VD-seislet transform for the ith slope pattern (corresponding to primaries or pegleg multiples of different orders), then, for any data vector $\mathbf{d}$,

$$\sum_{i=1}^{N} \|\mathbf{F}_i\,\mathbf{d}\|^2 = \sum_{i=1}^{N} \mathbf{d}^T\,\mathbf{F}_i^T\,\mathbf{F}_i\,\mathbf{d} = \sum_{i=1}^{N} \|\mathbf{d}\|^2 = N\,\|\mathbf{d}\|^2\;, \tag{11}$$

which means that all transforms taken together constitute a *tight frame* with constant N (Mallat, 2009).

Because of its overcompleteness, a frame representation for a given signal is not unique. In order to assure that different wavefield components do not leak into other parts of the frame, it is advantageous to employ sparsity-promoting inversion (Fomel and Liu, 2010). We use a nonlinear shaping-regularization scheme (Fomel, 2008) and define sparse decomposition as an iterative thresholding process (Daubechies et al., 2004)

$$\hat{\mathbf{f}}_{k+1} = \mathbf{S}[\mathbf{F}\,\mathbf{d} + (\mathbf{I} - \mathbf{F}\,\mathbf{B})\,\hat{\mathbf{f}}_k]\;, \tag{12}$$

$$\mathbf{f}_{k+1} = \mathbf{f}_k + \mathbf{F}\,\mathbf{d} - \mathbf{F}\,\mathbf{B}\hat{\mathbf{f}}_{k+1}\;, \tag{13}$$

where $\mathbf{f}_k$ are coefficients of the seislet frame at kth iteration, $\hat{\mathbf{f}}_k$ is an auxiliary quantity, $\mathbf{S}$ is a soft thresholding operator, $\mathbf{F}$ and $\mathbf{B}$ are frame construction and deconstruction operators

$$\mathbf{F} \equiv \left[\begin{array}{cccc} \mathbf{F}_1 & \mathbf{F}_2 & \cdots & \mathbf{F}_N \end{array}\right]^T\;, \tag{14}$$

$$\mathbf{B} \equiv \left[\begin{array}{cccc} \mathbf{F}_1^{-1} & \mathbf{F}_2^{-1} & \cdots & \mathbf{F}_N^{-1} \end{array}\right]\;. \tag{15}$$

The iteration in equations 12 and 13 starts with $\mathbf{f}_0 = \mathbf{0}$ and $\hat{\mathbf{f}}_0 = \mathbf{F}\mathbf{d}$ and is related to the linearized Bregman iteration (Cai et al., 2009), which converges to the solution of the constrained minimization problem:

$$\min_{\mathbf{f}} \|\mathbf{f}\|_1 \;s.t.\; \mathbf{B}\mathbf{f} = \mathbf{d}\;. \tag{16}$$

Separated wavefield can be calculated by $\mathbf{d}_i = \mathbf{B}\mathbf{M}_i\mathbf{f}_\eta$, where η is iteration number, masking operator $\mathbf{M}_i$ is a diagonal matrix as

$$\mathbf{M}_i = \begin{bmatrix} \mathbf{0} & \cdots & \cdots & \cdots & \cdots & \cdots & \mathbf{0} \\ \cdots & \cdots & \cdots & \cdots & \cdots & \cdots & \cdots \\ \mathbf{0} & \cdots & \mathbf{0} & \mathbf{0} & \mathbf{0} & \cdots & \mathbf{0} \\ \mathbf{0} & \cdots & \mathbf{0} & \mathbf{I}_{i,i} & \mathbf{0} & \cdots & \mathbf{0} \\ \mathbf{0} & \cdots & \mathbf{0} & \mathbf{0} & \mathbf{0} & \cdots & \mathbf{0} \\ \cdots & \cdots & \cdots & \cdots & \cdots & \cdots & \cdots \\ \mathbf{0} & \cdots & \cdots & \cdots & \cdots & \cdots & \mathbf{0} \end{bmatrix}_{N\times N}, \tag{17}$$

and $\mathbf{d}_i$ corresponds to the signal of interest (e.g., primaries or multiples of selected order). We calculate all patterns for primaries and multiples, and then apply sparse decomposition (equations 12 and 13) to separate primaries from multiples. In practice, a small number of iterations is usually sufficient for convergence and for achieving both model sparseness and data recovery.

SYNTHETIC DATA EXAMPLES

Validation of slope estimation and random noise elimination

A simple synthetic example is shown in Figure 1a. The synthetic data were generated by applying inverse NMO with time-varying velocities and represent perfectly hyperbolic events. Figure 1b shows local event slopes measured from the data using PWD algorithm (Fomel, 2002). PWD provides an accurate slope field for noise-free data. Figure 2a and 2b show the data after adding normally distributed random noise and local slopes from PWD, respectively. Compared with Figure 1b, PWD fails in finding exact slope field because of strong random noise. Next, we calculate slopes using NMO velocities from velocity scan. Picked NMO velocities (Figure 3a) are close to the exact velocity because velocity scan is less sensitive to strong random noise. As a consequence, VD slopes calculated from equation 7 provide a more accurate result (Figure 3b).

A direct application of the seislet transform is denoising. We apply both PWD-seislet and VD-seislet transforms on the noisy data (Figure 2a). Figure 4a and 4b show the transform coefficients of PWD-seislet and VD-seislet, respectively. The hyperbolic events are compressed in both transform domains. Notice that PWD-seislet coefficients get more concentrated at small scale than those of VD-seislet because parts of the random noise are also compressed along inaccurate PWD slopes. Meanwhile, random noise gets spread over different scales in the VD-seislet domain, while the predictable reflection information gets compressed to large coefficients at small scales, which makes signal and noise display different amplitude characteristics. Figure 4c shows a comparison between the decay of coefficients sorted from large to small in the PWD-seislet transform and the VD-seislet transform. Seislet transform can compress the seismic events with coincident wavelets, if the slopes of the reflections are

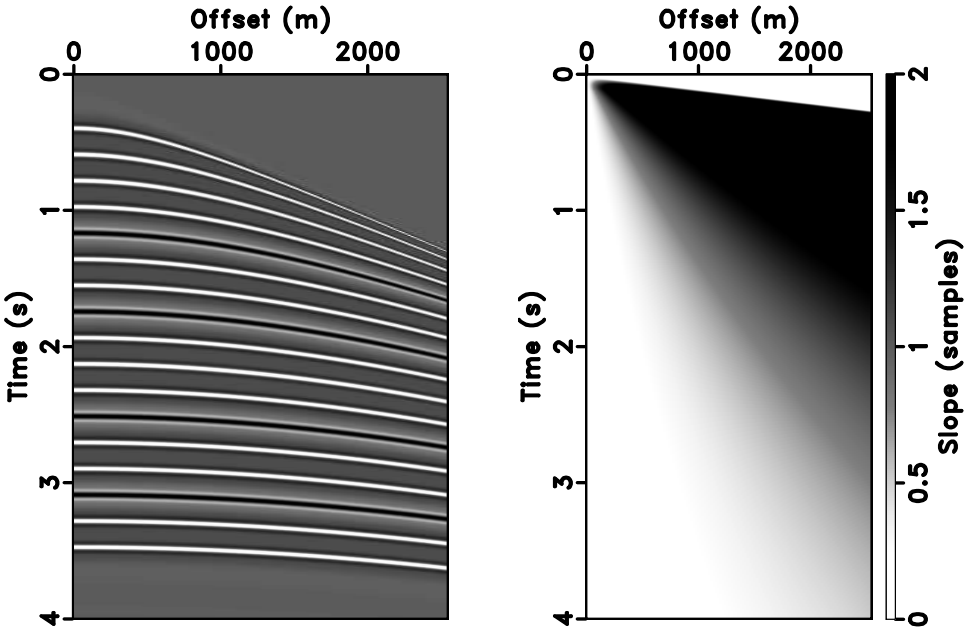

(a) (b)

Figure 1: Synthetic data (a) and slopes calculated by PWD (b).

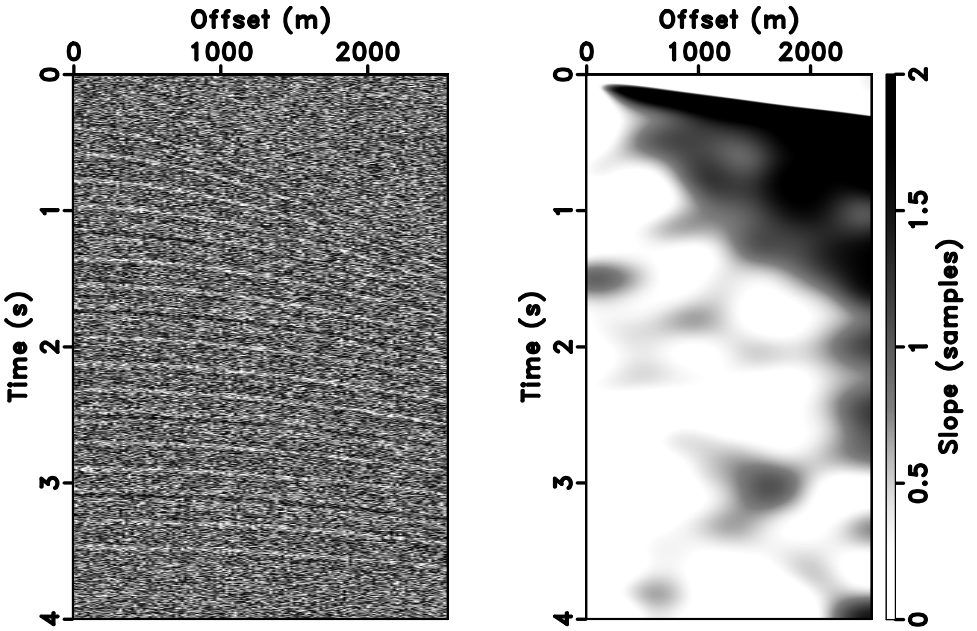

(a) (b)

Figure 2: Synthetic noisy data (a) and slopes calculated by PWD (b).

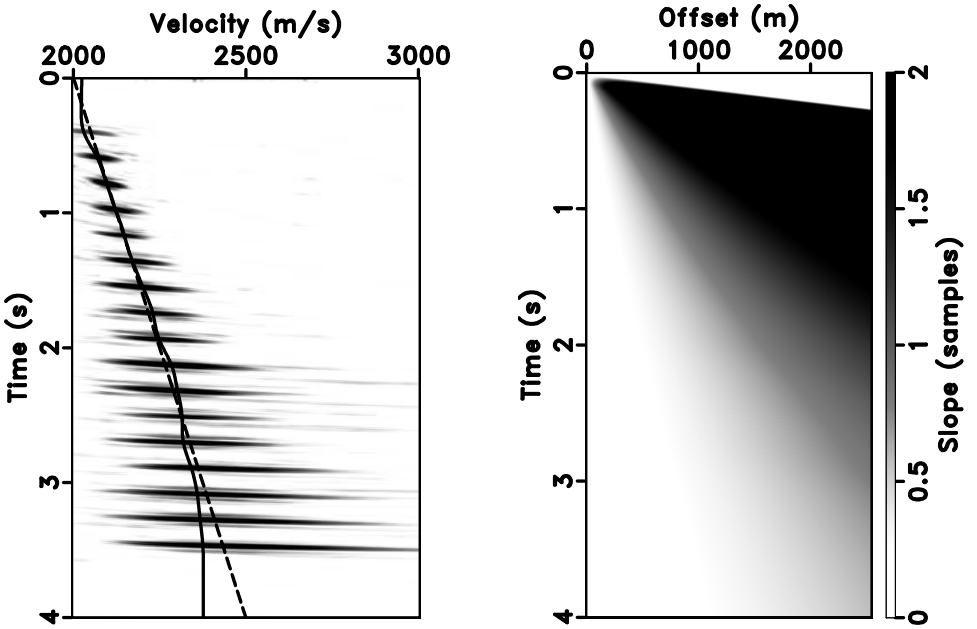

(a) (b)

Figure 3: Velocity scanning (dash line: exact velocity, solid line: picked velocity) (a) and VD slopes (b).

correct, the sparse large coefficients only correspond to the stacked reflection events. However, when the slopes of the reflections are not accurate, the stacked amplitude values for inconsistent wavelets will create more coefficients with smaller values. VD slopes are less affected by strong random noise than PWD slopes, which results in a faster decay of the VD-seislet coefficients. A simple thresholding method can easily remove the small coefficients of random noise. Figure 5a and 5b display the denoising results by using PWD-seislet transform and VD-seislet transform, respectively. The events after PWD-seislet transform denoising show serious distortion while VD-seislet transform produces a reasonable denoising result. For numerically comparison, we use the signal-to-noise ratio (SNR) defined as $SNR = 10\log_{10}\frac{||\mathbf{s}||_2^2}{||\mathbf{s}-\hat{\mathbf{s}}||_2^2}$, where $\mathbf{s}$ is the noise-free signal and $\hat{\mathbf{s}}$ is the denoised signal. The original SNR of the noisy data (Figure 2a) is -12.53 dB. The SNR of the denoised results using the PWD-seislet transform (Figure 5a) and the VD-seislet transform (Figure 5b) are 0.53 dB and 1.94 dB, respectively.

Separation of primaries and pegleg multiples

Next, we use a synthetic CMP gather (Figure 6a) to test separation of primaries and pegleg multiples by VD-seislet frame. This gather was generated by Lumley et al. (1994) using Haskell-Thompson elastic modeling and a well log from the Mobil AVO dataset (Keys and Foster, 1998). The gather contains primaries and water-bottom

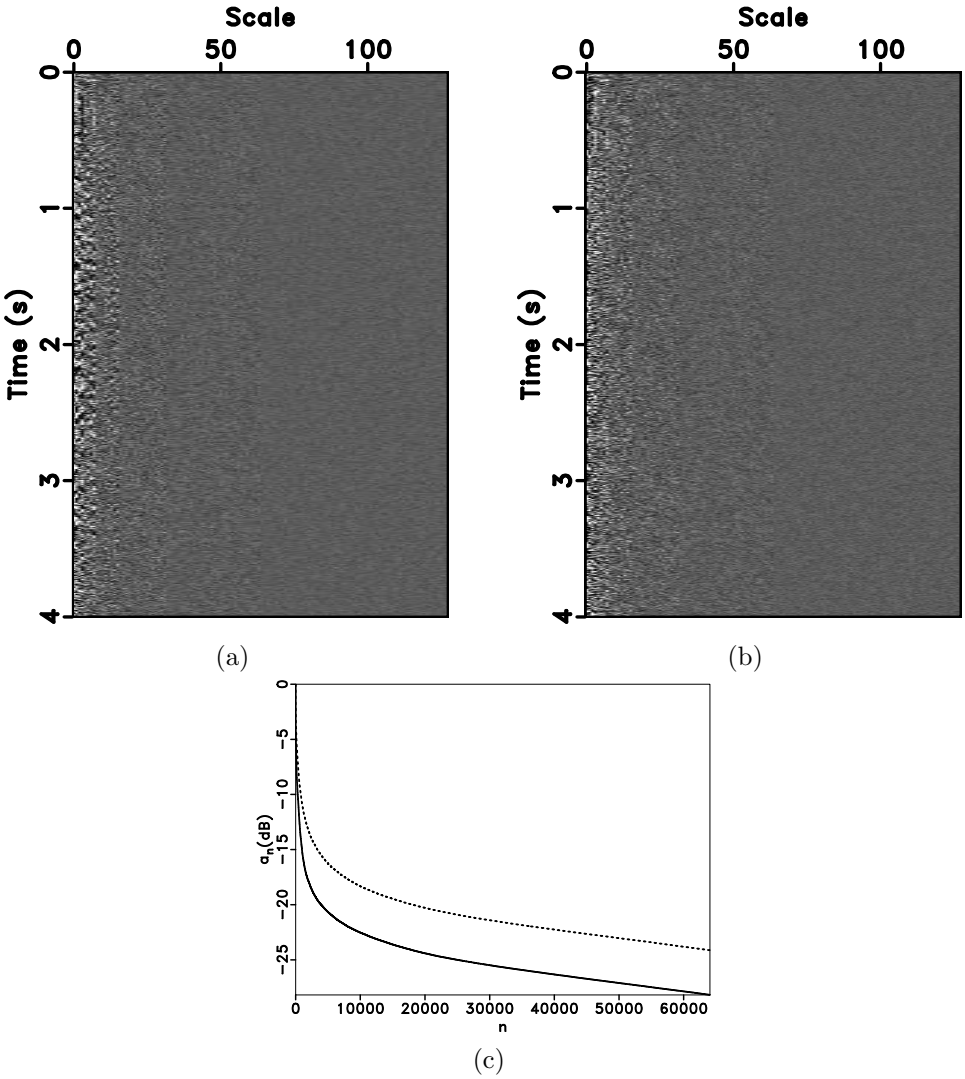

Figure 4: PWD-seislet coefficients (a), VD-seislet coefficients (b), and transform coefficients sorted from large to small, normalized, and plotted on a decibel scale (Solid line - VD-seislet transform. Dashed line - PWD-seislet transform) (c).

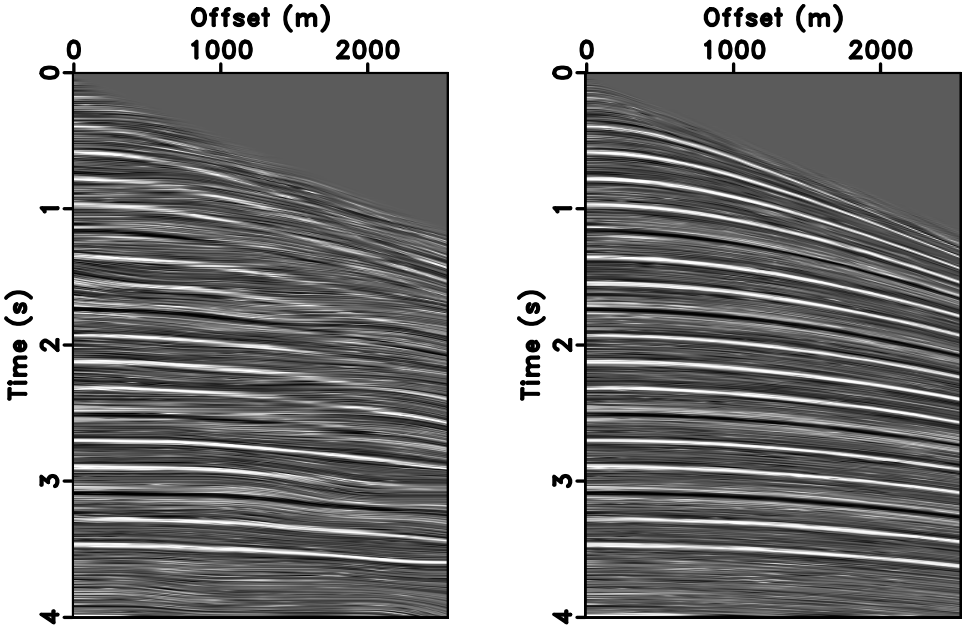

(a) (b)

Figure 5: Denoising result using different transforms. PWD-seislet transform (a) and VD-seislet transform (b).

multiples of different orders.

To separate pegleg multiples from primaries, we transform the data using VD-seislet frame by involving different VD slope fields (Figure 7a) according to equations 7 and 10. The primary velocities and calculated velocities of different-order pegleg multiples are shown in Figure 6b. The estimated curves of multiple velocities indicate accurate trends in velocity spectra. We use a nonlinear shaping-regularization scheme (equations 12-13) to separate different wavefield components, which are shaped to be sparse in the corresponding VD-seislet frame domain (Figure 7b). In this example, the pattern number in equation 11 N is selected to be 4. The separated wavefields are shown in Figure 8 and display reasonably accurate separation results.

FIELD DATA EXAMPLES

We test VD-seislet denoising by employing a field land data provided by Geofizyka Torun Sp. Z.o.o, Poland from FreeUSP website*. Figure 9a show the CMP gathers after removing most of ground roll. The strong random noise makes reflection events hardly visible. However, velocity analysis from equation 6 can still produce a reasonable velocity field. Equation 7 converts RMS velocity to seismic pattern (Figure 9b), which displays the hyperbolic slopes from negative to positive in CMP gathers and

*http://www.freeusp.org/RaceCarWebsite/TechTransfer/Tutorials/Processing_2D

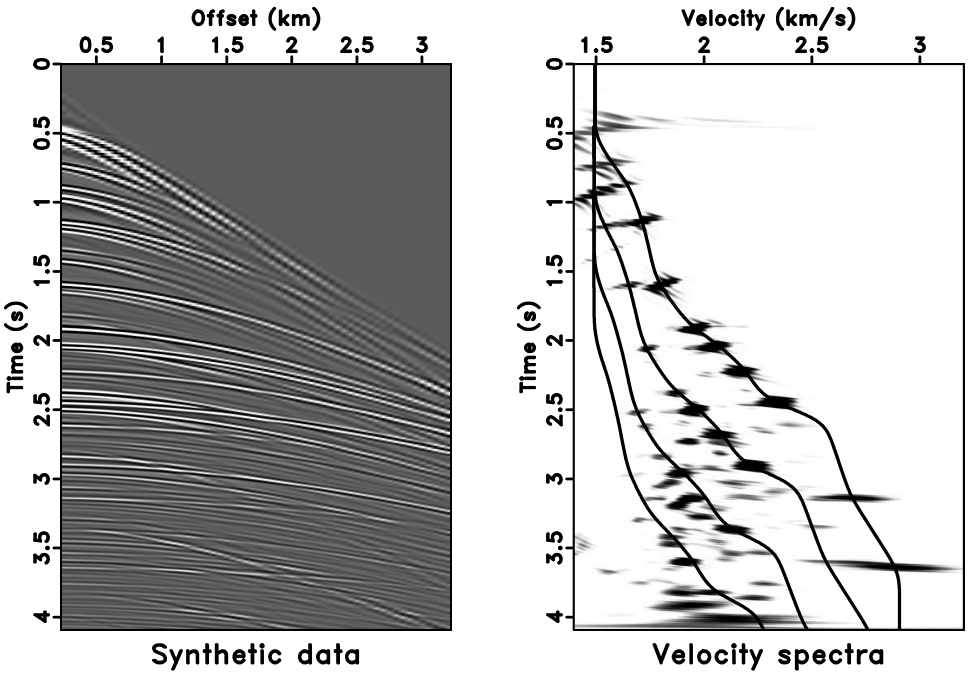

(a) (b)

Figure 6: Synthetic model (a) and velocity trends of primaries and multiples (b).

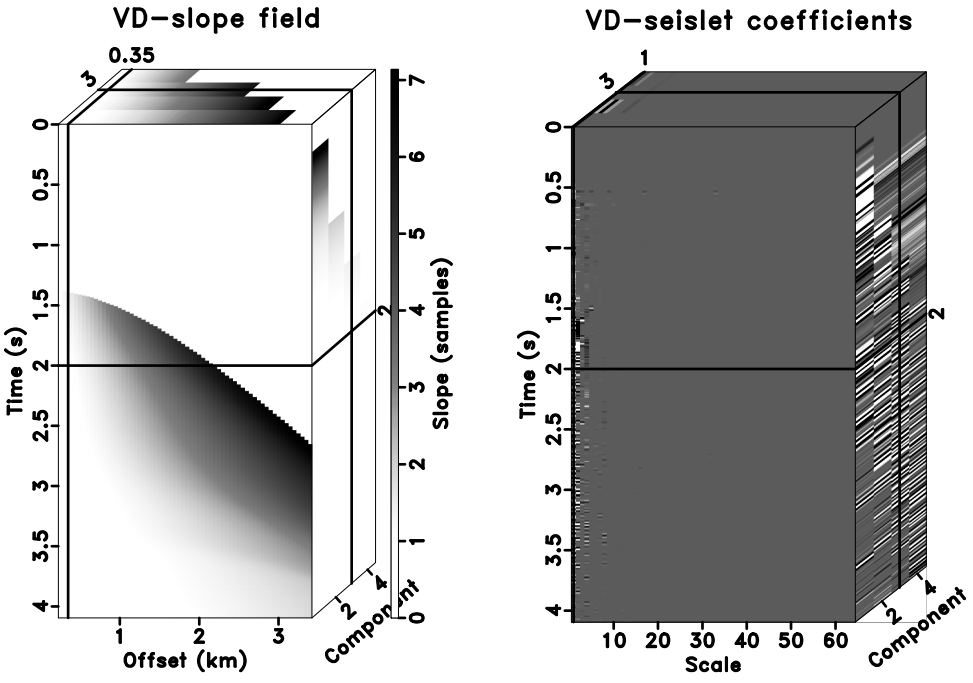

(a) (b)

Figure 7: VD slopes (a) and VD-seislet coefficients (b).

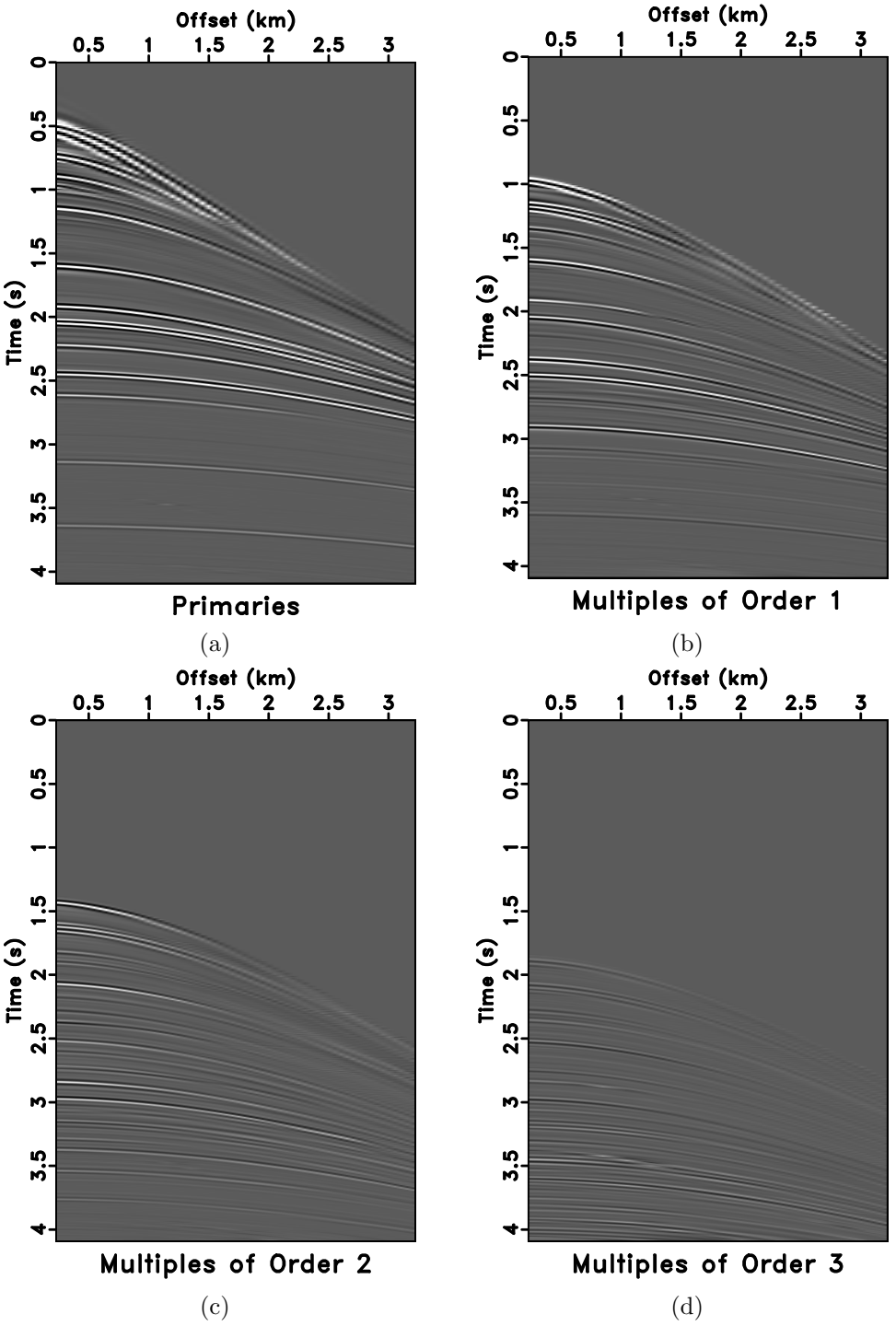

Figure 8: Separated wavefields. Primaries (a), first-order multiples (b), second-order multiples (c), and third-order multiples (d).

varying slopes in common-offset section. VD-seislet transform utilizes the slopes to compress reflections along offset axis. Figure 9c shows the VD-seislet coefficients, in which the small dynamic range of seislet coefficients implies a good compression ratio. If we choose the significant coefficients at the coarse scale, e.g., scale < 8, and zero out difference coefficients at the finer scales, the inverse transform effectively removes incoherent noise from the gathers (Figure 9d).

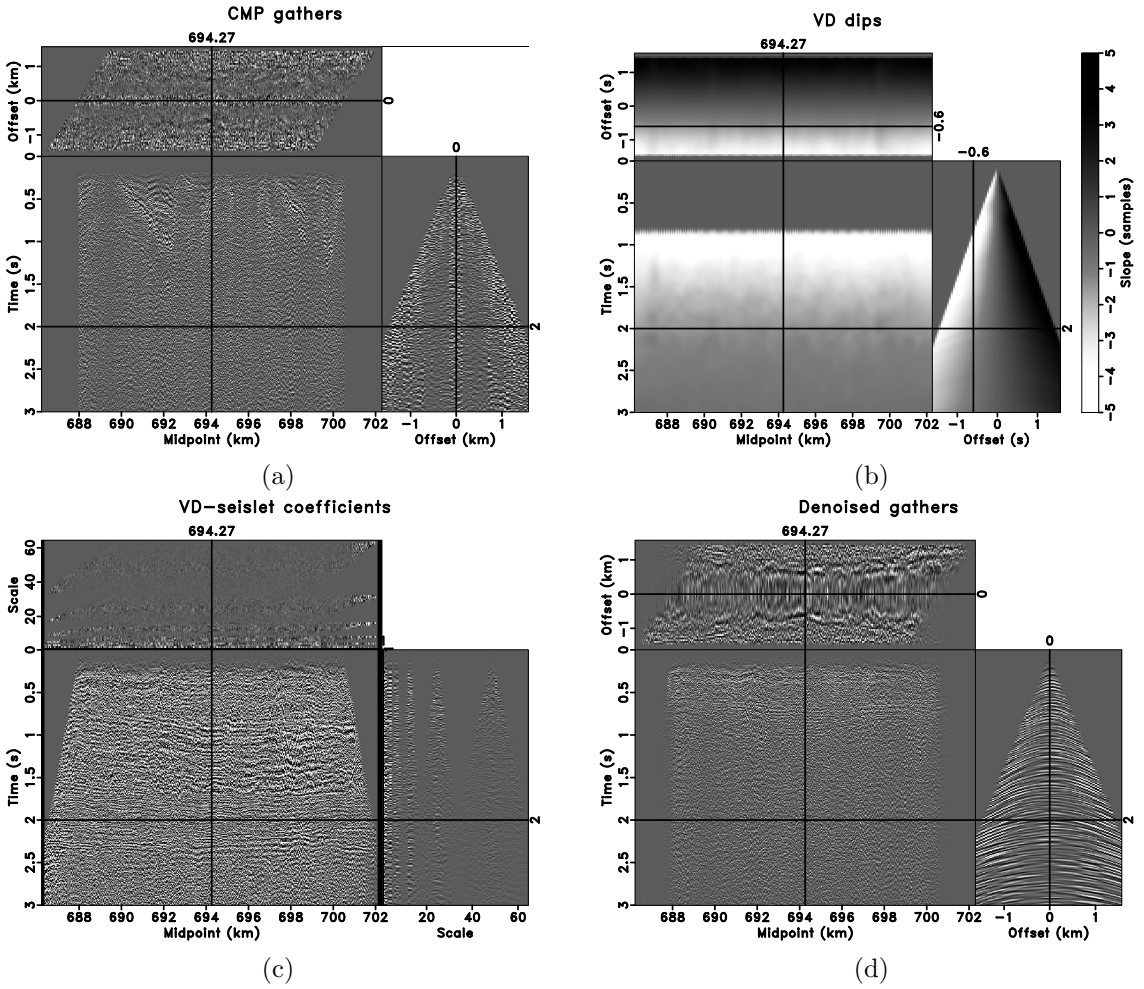

Figure 9: Field CMP gathers (a), VD slopes (b), VD-seislet coefficients (c), and denoising result using VD-seislet transform (b).

Next, we test the proposed algorithm to separate multi-wavefields on a single CMP gather from the Viking Graben (Mobil AVO) dataset (Keys and Foster, 1998). The field data are shown in Figure 10a. We pick the primary velocities by muting spectra energy of multiples. Multiple RMS velocities with different orders (equation 9) follow the pseudo-primary NMO equation 8. The velocity spectra of primaries and multiples are shown in Figure 10b. Equations 7 and 10 convert velocities to slopes, which help the VD-seislet frame separate primaries from different-order pegleg multiples (we only display three orders). Figure 11 displays the separated primaries and different-order multiples. The corresponding velocity spectra are shown in Figure 12.

After separating different wavefields, the velocity spectra confirm that the signals get concentrated around their respective trends.

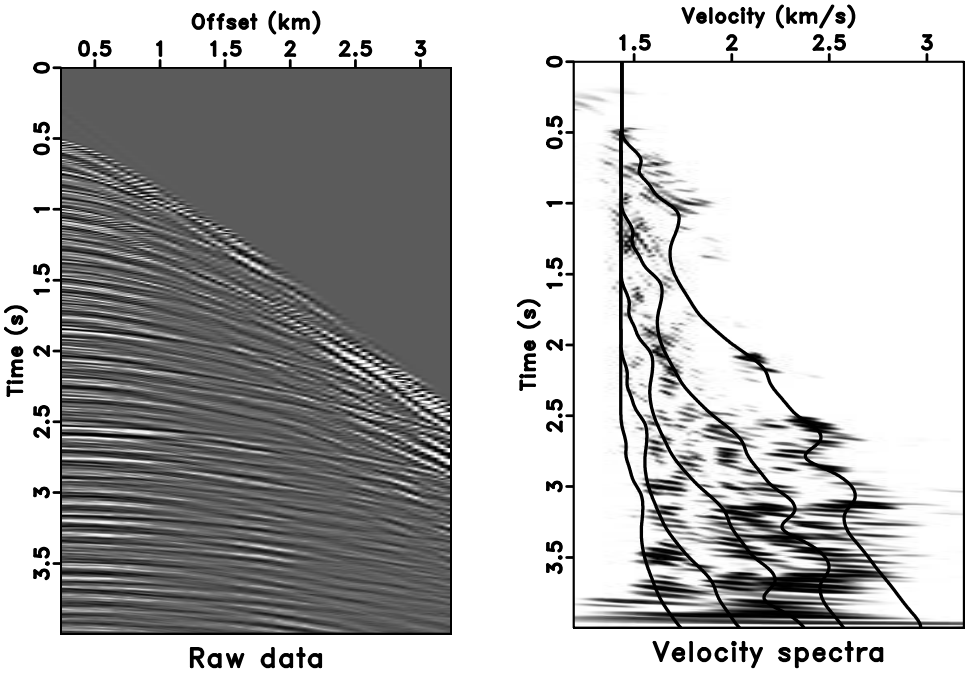

Figure 10: Field CMP gather (a) and velocity trends of primaries and multiples (b).

DISCUSSION

What are the limitations of the proposed algorithms? First, VD-seislet transform may have difficulties in dealing with nonhyperbolic moveouts. However, it is possible to extend it to nonhyperbolic moveout equation (Casasanta and Fomel, 2011), which would provide the possibility to handle large offsets and anisotropy (Fomel and Grechka, 2001). Compared with PWD-seislet transform, VD-seislet transform provides more accurate representation for seismic events with class II AVO anomalies (Rutherford and Williams, 1989) that cause seismic amplitudes to go through a polarity reversal by using advanced velocity analysis, e.g., AB semblance (Sarkar et al., 2001, 2002; Fomel, 2009b). Finally, the proposed method works best for the relatively deep water situations where primaries and multiples are well separated.

CONCLUSIONS

We have introduced the VD-seislet transform, a new domain for analyzing prestack reflection data in CMP domain. The new transform is able to compress reflection data away from strong random noise. In this formulation, the normal moveout

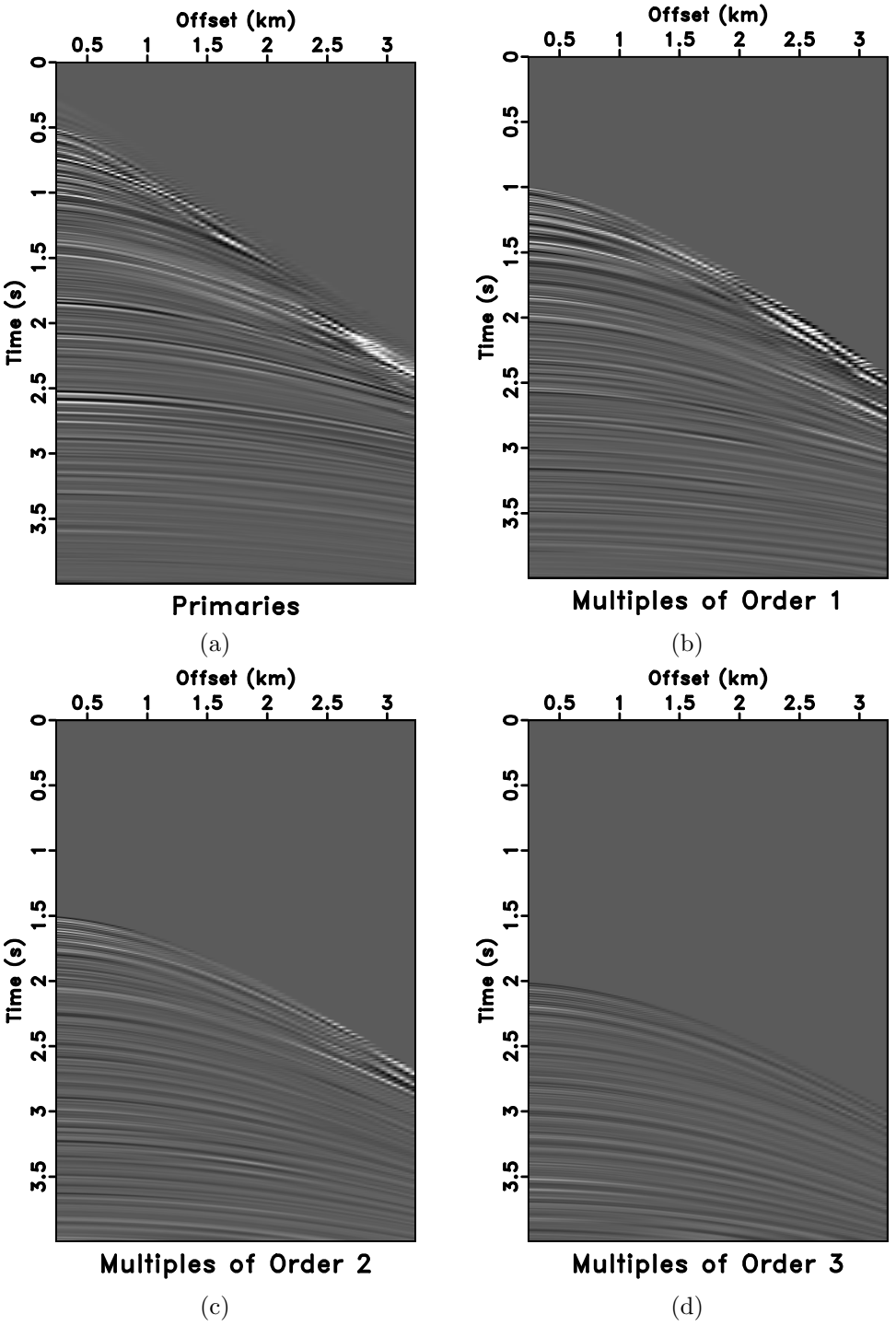

Figure 11: Separated wavefields. Primaries (a), first-order multiples (b), second-order multiples (c), and third-order multiples (d).

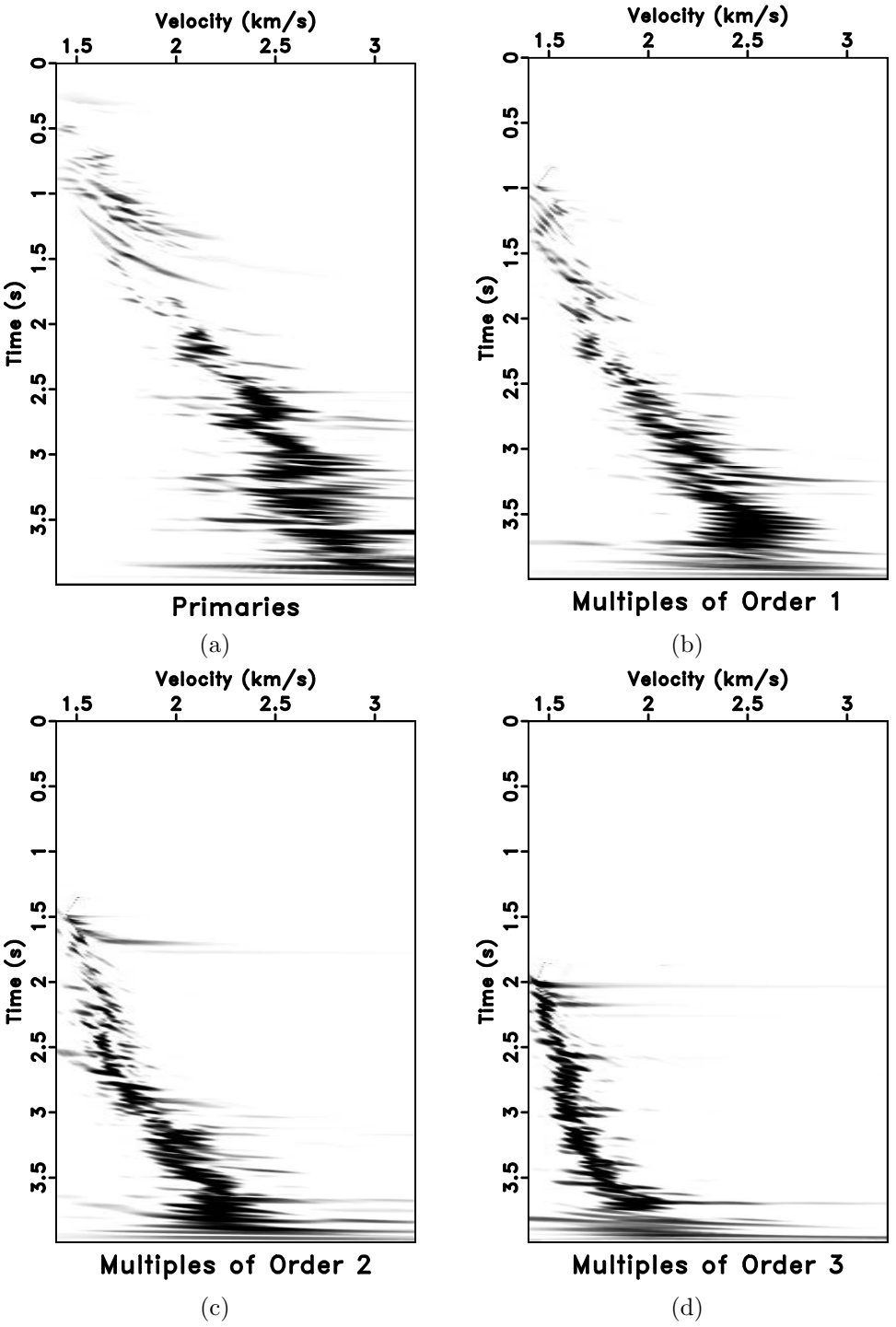

Figure 12: Velocity spectra of different wavefields. Primaries (a), first-order multiples (b), second-order multiples (c), and third-order multiples (d).

equation serves as a bridge between local slopes and scanned velocities that are not sensitive to strong random noise and aliasing. We also used the explicit relationship between slopes and velocities of primary and multiple events to extend VD-seislet transform to a VD-seislet frame. We have shown example applications of VD-seislet transform to signal and noise separation. Other traditional processing tasks such as data interpolation can be also easily defined in the VD-seislet domain.

ACKNOWLEDGMENTS

We thank Valentina Socco, Adriana Citlali Ramirez, and three anonymous reviewers for helpful suggestions, which improved the quality of the paper. This work is partly supported by National Natural Science Foundation of China (Grant No. 41430322 and 41274119) and 863 Programme of China (Grant No. 2012AA09A2010). All results are reproducible in the Madagascar open-source software environment (Fomel et al., 2013).

APPENDIX: THE LIFTING SCHEME FOR DWT

The lifting scheme (Sweldens, 1995) provides a convenient approach for defining wavelet transforms by breaking them down into the following steps:

1. Divide data into even and odd components, $\mathbf{e}$ and $\mathbf{o}$.
2. Find a residual difference, $\mathbf{r}$, between the odd component and its prediction from the even component:
$$\mathbf{r} = \mathbf{o} - \mathbf{P}[\mathbf{e}] \ , \tag{A-1}$$
where $\mathbf{P}$ is a *prediction* operator.
3. Find a coarse approximation, $\mathbf{c}$, of the data by updating the even component:
$$\mathbf{c} = \mathbf{e} + \mathbf{U}[\mathbf{r}] \ , \tag{A-2}$$
where $\mathbf{U}$ is an *update* operator.
4. The coarse approximation, $\mathbf{c}$, becomes the new data, and the sequence of steps is repeated at the next scale.

The Cohen-Daubechies-Feauveau (CDF) 5/3 biorthogonal wavelets (Cohen et al., 1992) are constructed by making the prediction operator a linear interpolation between two neighboring samples,

$$\mathbf{P}[\mathbf{e}]_k = \left(\mathbf{e}_{k-1} + \mathbf{e}_k\right)/2 \ , \tag{A-3}$$

and by constructing the update operator to preserve the running average of the signal (Sweldens and Schröder, 1996), as follows:

$$\mathbf{U}[\mathbf{r}]_k = (\mathbf{r}_{k-1} + \mathbf{r}_k)/4 \ . \tag{A-4}$$

Furthermore, one can create a high-order CDF 9/7 biorthogonal wavelet transform by using CDF 5/3 biorthogonal wavelets twice with different lifting operator coefficients (Lian et al., 2001). The transform is easily inverted according to reversing the steps above:

1. Start with the coarsest scale data representation **c** and the coarsest scale residual **r**.

2. Reconstruct the even component **e** by reversing the operation in equation A-2, as follows:
$$\mathbf{e} = \mathbf{c} - \mathbf{U}[\mathbf{r}] \ , \tag{A-5}$$

3. Reconstruct the odd component **o** by reversing the operation in equation A-1, as follows:
$$\mathbf{o} = \mathbf{r} + \mathbf{P}[\mathbf{e}] \ , \tag{A-6}$$

4. Combine the odd and even components to generate the data at the previous scale level and repeat the sequence of steps.

REFERENCES

Berkhout, A. J., and D. J. Verschuur, 1997, Estimation of multiple scattering by iterative inversion, Part 1 Theoretical consideration: Geophysics, **62**, 1586–1595.

———, 2006, Imaging of multiple reflections: Geophysics, **71**, no. 4, SI209–SI220.

Brown, M. P., and A. Guitton, 2005, Least-squares joint imaging of multiples and primaries: Geophysics, **70**, no. 5, S79–S89.

Burnett, W., and S. Fomel, 2009, Moveout analysis by time-warping: 79nd Annual International Meeting, SEG, Expanded Abstracts, 3710–3714.

Cai, J., S. Osher, and Z. Shen, 2009, Linearized Bregman iterations for compressed sensing: Mathematics of Computation, **78**, 1515–1536.

Canales, L. L., 1984, Random noise reduction: 54th Annual International Meeting, SEG, Expanded Abstracts, Session: S10.1.

Casasanta, L., and S. Fomel, 2011, Velocity-independent τ-p moveout in a vertically-varying VTI medium: Geophysics, **76**, no. 4, U45–U57.

Chauris, H., and T. Nguyen, 2008, Seismic demigration/migration in the curvelet domain: Geophysics, **73**, no. 2, S35–S46.

Chen, Z., S. Fomel, and W. Lu, 2013a, Accelerated plane-wave destruction: Geophysics, **78**, no. 1, V1–V9.

———, 2013b, Omnidirectional plane-wave destruction: Geophysics, **78**, no. 5, V171–V179.

Claerbout, J. F., 1992, Earth Soundings Analysis: Processing Versus Inversion: Blackwell Scientific Publications.

Cohen, A., I. Daubechies, and J. Feauveau, 1992, Biorthogonal bases of compactly supported wavelets: Communications on Pure and Applied Mathematics, **45**, 485–560.

Daubechies, I., M. Defries, and C. D. Mol, 2004, An iterative thresholding algorithm for linear inverse problems with a sparsity constraint: Communications on Pure and Applied Mathematics, **LVII**, 1413–1457.

Dix, C. H., 1955, Seismic velocity from surface measurement: Geophysics, **20**, 68–86.

Fomel, S., 2002, Applications of plane-wave destruction filters: Geophysics, **67**, 1946–1960.

———, 2006, Towards the seislet transform: 76nd Annual International Meeting, SEG, Expanded Abstracts, 2847–2851a.

———, 2007, Velocity-independent time-domain seismic imaging using local event slopes: Geophysics, **72**, no. 3, S139–S147.

———, 2008, Nonlinear shaping regularization in geophysical inverse problems: 78th Annual International Meeting, SEG, Expanded Abstracts, 2046–2051.

———, 2009a, Adaptive multiple subtraction using regularized nonstationary regression: Geophysics, **74**, no. 1, V25–V33.

———, 2009b, Velocity analysis using AB semblance: Geophysical Prospecting, **57**, 311–321.

———, 2010, Predictive painting of 3D seismic volumes: Geophysics, **75**, no. 4, A25–A30.

Fomel, S., and V. Grechka, 2001, Nonhyperbolic reflection moveout of P waves. An overview and comparison of reasons, *in* CWP-372: Colorado School of Mines.

Fomel, S., and A. Guitton, 2006, Regularizing seismic inverse problems by model reparameterization using plane-wave construction: Geophysics, **71**, no. 5, A43–A47.

Fomel, S., and Y. Liu, 2010, Seislet transform and seislet frame: Geophysics, **75**, no. 3, V25–V38.

Fomel, S., P. Sava, I. Vlad, Y. Liu, and V. Bashkardin, 2013, Madagascar: open-source software project for multidimensional data analysis and reproducible computational experiments: Journal of Open Research Software, **1**, e8.

Foster, D. J., and C. C. Mosher, 1992, Suppression of multiple reflections using the Radon transform: Geophysics, **57**, 386–395.

Guitton, A., and D. Verschuur, 2004, Adaptive subtraction of multiples using the L1-norm: Geophysical Prospecting, **52**, 27–38.

Hargreave, N., B. verWest, R. Wombell, and D. Trad, 2003, Multiple attenuation using an apex-shifted Radon transform: 73rd Annual International Meeting, SEG, Expanded Abstracts, 1929–1932.

Herrmann, F., D. Wang, D. Hennenfent, and P. Moghaddam, 2008, Curvelet-based seismic data processing: a multiscale and nonlinear approach: Geophysics, **73**, no. 1, A1–A5.

Herrmann, P., T. Mojesky, M. Magesan, and P. Hugonnet, 2000, De-aliased, high-resolution radon transforms: Society of Exploration Geophysicists 70th Annual International Meeting, SP2, 1953–1956.

Hunt, L., P. Gary, and W. Upham, 1996, The impact of an improved radon transform on multiple attenuation: 66th Annual International Meeting, SEG, Expanded Abstracts, 1535–1538.

Jensen, A., and A. la Cour-Harbo, 2001, Ripples in mathematics: the discrete wavelet transform: Springer.

Karsli, H., D. Dondurur, and G. Çifçi, 2006, Application of complex-trace analysis to seismic data for random-noise suppression and temporal resolution improvement: Geophysics, **71**, no. 3, V79–V86.

Keys, R. G., and D. J. Foster, 1998, Comparison of seismic inversion methods on a single real data set: Society of Exploration Geophysicists.

Lian, C., K. Chen, H. Chen, and L. Chen, 2001, Lifting based discrete wavelet transform architecture for JPEG2000: The 2001 IEEE International Symposium on Circuits and Systems, IEEE, II445–II448.

Liu, Y., and S. Fomel, 2010, OC-seislet: Seislet transform construction with differential offset continuation: Geophysics, **75**, no. 6, WB235–WB245.

Liu, Y., and C. Liu, 2013, Velocity-dependent seislet transform and its applications: 83rd Annual International Meeting, SEG, Expanded Abstracts, 3661–3666.

Liu, Y., N. Liu, and C. Liu, 2015, Adaptive prediction filtering in t-x-y domain for random noise attenuation using regularized nonstationary autoregression: Geophysics, **80**, no. 1, V13–V21.

Lu, W., and J. Liu, 2007, Random noise suppression based on discrete cosine transform: 77th Annual International Meeting, SEG, Expanded Abstracts, 2668–2672.

Lumley, D., D. Nichols, and T. Rekdal, 1994, Amplitude-preserved multiple suppression: Stanford Exploration Project, **SEP report 82**, 25–45.

Mallat, S., 2009, A wavelet tour of signal processing: The sparse way: Academic Press.

Neelamani, R., A. I. Baumstein, D. G. Gillard, M. T. Hadidi, and W. I. Soroka, 2008, Coherent and random noise attenuation using the curvelet transform: The Leading Edge, **27**, 240–248.

Ottolini, R., 1983a, Signal/noise separation in dip space: Stanford Exploration Project, **SEP report 37**, 143–149.

———, 1983b, Velocity independent seismic imaging: Stanford Exploration Project, **SEP report 37**, 59–68.

Reiter, E. C., M. N. Toksöz, T. H. Keho, and G. M. Purdy, 1991, Imaging with deep-water multiples: Geophysics, **56**, 1081–1086.

Ristau, J. P., and W. M. Moon, 2001, Adaptive filtering of random noise in 2-D geophysical data: Geophysics, **66**, 342–349.

Rutherford, S. R., and R. H. Williams, 1989, Amplitude-versus-offset variations in gas sands: Geophysics, **54**, 680–688.

Sacchi, M., and H. Kuehl, 2001, ARMA formulation of FX prediction error filters and projection filters: Journal of Seismic Exploration, **9**, 185–197.

Sacchi, M., and M. Naghizadeh, 2009, Adaptive linear prediction filtering for random noise attenuation: 79th Annual International Meeting, SEG, Expanded Abstracts, 3347–3351.

Sacchi, M. D., and T. J. Ulrych, 1995, High-resolution velocity gathers and offset

space reconstruction: Geophysics, **60**, 1169–1177.

Sarkar, D., R. T. Baumel, and K. L. Larner, 2002, Velocity analysis in the presence of amplitude variation: Geophysics, **67**, 1664–1672.

Sarkar, D., J. P. Castagna, and W. Lamb, 2001, AVO and velocity analysis: Geophysics, **66**, 1284–1293.

Schleicher, J., J. C. Costa, L. T. Santos, A. Novais, and M. Tygel, 2009, On the estimation of local slopes: Geophysics, **74**, no. 4, P25–P33.

Sweldens, W., 1995, The lifting scheme: A new philosophy in biorthogonal wavelet constructions: Wavelet Applications in Signal and Image Processing III, **Proc. SPIE 2569**, 68–79.

Sweldens, W., and P. Schröder, 1996, Building your own wavelets at home, *in* Wavelets in Computer Graphics: ACM SIGGRAPH Course notes, 15–87.

Trad, D., T. Ulrych, and M. Sacchi, 2003, Latest views of the sparse radon transform: Geophysics, **68**, 386–399.

Verschuur, D. J., A. J. Berkhout, and C. P. A. Wapenaar, 1992, Adaptive surface-related multiple elimination: Geophysics, **57**, 1166–1177.

Wang, Y., 2003a, Multiple attenuation: coping with the spatial truncation effect in the Radon transform domain: Geophysical Prospecting, **51**, 75–83.

———, 2003b, Multiple subtraction using an expanded multichannel matching filter: Geophysics, **68**, 346–354.

Weglein, A. B., F. A. Gasparotto, P. M. Carvalho, and R. H. Stolt, 1997, An inverse-scattering series method for attenuating multiples in seismic reflection data: Geophysics, **62**, 1975–1989.

Youn, O. K., and H. W. Zhou, 2001, Depth imaging with multiples: Geophysics, **66**, 246–255.

Zhou, B., and S. Greenhalgh, 1996, Multiple suppression by 2D filtering in the parabolic τ-p domain: a wave-equation-based method: Geophysical Prospecting, **44**, 375–401.